


Article

An Investigation into the Future Changes in Onset and Cessation of Rain and Their Variability over the Aswa Catchment, Uganda

Michael Iwadra ^{1,2,*} , P. T. Odirile ¹, B. P. Parida ¹ and D. B. Moalafhi ³

¹ Faculty of Engineering and Technology, University of Botswana, Gaborone P/Bag 0061, Botswana; odirilep@mopipi.ub.bw (P.T.O.); paridab@mopipi.ub.bw (B.P.P.)

² Department of Agricultural and Bio Systems Engineering, Makerere University, Kampala P.O. box 7062, Uganda

³ Department of Environmental Science, Faculty of Science, University of Botswana, Gaborone P/Bag 0022, Botswana; moalafhid@mopipi.ub.bw

* Correspondence: miwadra@caes.mak.ac.ug or miwadra@yanoo.co.uk

Received: 28 April 2020; Accepted: 19 May 2020; Published: 29 May 2020



Abstract: Future global warming may result in extreme precipitation events leading to crop, environment and infrastructure damage. Rainfall is a major input for the livelihood of peasant farmers in the Aswa catchment where the future rainfall variability, onset and cessation are also likely to be affected. The Aswa catchment has limited rainfall data; therefore, use of secondary datasets from Tropical Rainfall Measuring Mission (TRMM) is considered in this study, based on the close correlation of the recorded and TRMM rainfall. The latter was used to calibrate the statistical downscaling model for downscaling of two general circulation models to simulate future changes in rainfall. These data were analyzed for trends, wet and dry conditions/variability; onset and cessations of rain using the Mann–Kendall test, Standardized Precipitation Index (SPI) and the cumulative percentage mean rainfall method, respectively. Results show future rainfall is likely to increase, accompanied by increasing variability reaching as high as 118.5%. The frequency of SPI values above 2 (extreme wetness) is to increase above current level during mid and end of the century. The highest rainfall variability is expected especially during the onset and cessation months, which are generally expected to come earlier and later, by up to four and five weeks, respectively. The reliability worsens from the midterm (2036–2065) to long term (2066–2099). These likely changes in rainfall quantities, variability, onset and cessation months are some of the key rainfall dynamics that have implications for future arable agriculture, environment and water resource availability and planning over the Aswa catchment, as is increasingly the case elsewhere.

Keywords: SDSM; SPI; mann–kendall; rainfall variability; rainfall onset and cessation

1. Introduction

Projected future global warming may result in extreme precipitation events causing drought and flooding, which in turn may result in crop yield reduction, increased soil erosion and damage to infrastructure [1–5]. The recent report by the Intergovernmental Panel on Climate Change (IPCC) [6] indicates that global warming above pre-industrial levels (1900) of 1.5 °C and beyond would have adverse impacts on communities that depend on agriculture in the least developed countries. Rainfall is key to livelihoods of peasant farmers who depend on rain fed agriculture [7–11]. Declines in rainfall, increased variability and/or uncertainty would increase the risk of hunger and poverty especially for the peasantry. Fishman [12] argues that an increase in rainfall variability amidst increased annual rainfall overrules the benefit expected from the increase on crop yields. Increased future rainfall

variability is, therefore, a great concern for the socio-economic wellbeing of the communities living in Aswa catchment and other areas with similar climatic conditions.

Over the country of Uganda as a whole, more than 72 % of the economically active population derive their livelihood from agriculture, which contributes about 24.6 % of the Gross Domestic Product (GDP) [13]. The study area of Aswa catchment offers a typical Ugandan and African setting where the future socio-economic wellbeing of the community who mostly depend on agriculture is uncertain due to impacts of climate change. More than two million people, of which more than 70% are peasants, live in the Aswa catchment [14,15]. The catchment is characterized by periodic and extended drought spells, leading to chronic food insecurity and famine. With an annual population growth rate of over 3%, and within the context of climate change, the future is increasingly becoming more uncertain. Detailed research on variability in the future rainfall changes and their onset and cessation at the catchment and local level is, therefore, required for effective crop, environment and water resource planning and management.

The Aswa catchment also lacks adequate recorded climate data, as is generally the case across most of the African continent and other developing countries in the world. This challenge, among others, could be addressed by using secondary data, such as the Tropical Rainfall Measuring Mission (TRMM) [15,16]. Such data can be used to downscale General Circulation Models (GCMs) to appropriate local catchment resolutions. GCMs are used to project changes in climatic parameters, such as rainfall under various climate change Representative Concentration Pathway (RCP) scenarios, defined by the Intergovernmental Panel for Climate Change (IPCC). However, these projections are defined at coarse grid resolutions at which the GCMs are configured and, thus, being unable to resolve important sub-grid scale variations. Therefore, the GCMs cannot be used directly for climate change impact studies of small catchments such as Aswa; thus, downscaling is required to generate corresponding data. In addition to GCMs not providing catchment scale information, despite being our major source of knowledge about the future, they can also provide biased information [17,18].

For downscaling GCMs, two downscaling methods, dynamical and statistical, are available. Other nonlinear methods using artificial neural network (ANN) are also being used lately [19,20] for generating long-term rainfall patterns. Statistical Downscaling (SD) is usually preferred over dynamical downscaling as the former produces local weather and climatic time series, which is cheap, readily transferable and computationally less demanding by use of appropriate statistical or empirical relationships with predictor variables and, therefore, has been widely used in climate change studies [21]. Products of statistical downscaling can be limited when there are some systematic errors in input data used to calibrate the downscaling model, however. Systematic biases for the current climate are also unavoidable in GCMs [22]. The biases can be propagated through the downscaling process with far reaching implications on the simulations and any subsequent applications [23,24]. The first step towards reducing the bias and improving the simulations is usually to avoid using unrealistic or inaccurate datasets for calibrating the downscaling. In this regard input data used for downscaling can either be bias corrected before downscaling or the simulations are bias corrected themselves after downscaling [17,24]. Caution is also needed during post processing of the simulations to keep minimal chances that the original climate change signal could be affected as this alteration can substantially affect impact model results [25]. Depending on the level of biasness of downscaled products from observations and the intended use of the products, on a case-by-case basis, bias correction may not be critical.

In Statistical Down Scaling Model (SDSM), a combination of Multiple Linear Regression (MLR) and the Stochastic Weather Generator (SWG) is used for generating climate scenarios for assessment of various parameters of the data [21,26]. This study therefore, uses secondary rainfall data (TRMM) to calibrate SDSM in a downscaling experiment of two General Circulation Models (GCMs)—Hadley Centre Coupled Model version 3 (HadCM3) and Canadian Earth System Model (CanESM2)—for simulation of future rainfalls for the data-constrained, but socio-economically important Aswa catchment located in Uganda, within the context of changing climate, as reported in previous

studies [15]. The projected future rainfall is analyzed, using various methods, for changes in variability, onset and cessation. These changes are expected to have a profound impact on socio-economic wellbeing of the farmers and the environment particularly in Aswa catchment, as well as areas and regions that have similar climatic and socio-economic environment.

2. Materials and Methods

2.1. Study Site

The Aswa River catchment, at its confluence with River Nile, lies mainly in the northeastern part of Uganda with a small portion extending into South Sudan. The total catchment area spreads over 31,000 km² and lies between 31.9° E–34.25° E latitude and 2.05° N–4.09° N longitude. Figure 1 shows the location of the catchment area and the points from which TRMM data were downloaded. Coordinates of the TRMM data locations are shown in Table 1. The catchment has a wide range of annual rainfall amounts and distribution pattern. The northeastern parts have a semi-arid climate with annual rainfall varying between 500 and 800 mm, while the western and southern parts have semi-humid and humid climate with annual rainfall ranging from 800 to more than 1400 mm in some places.

Table 1. TRMM rainfall data location points.

Location	Latitude, °N	Longitude, °E
Agoro	3.88	33.13
Agago	2.88	33.38
Amuria	2.13	33.63
Kaabong	3.63	33.88
Kitgum	3.38	32.88
Gulu	2.63	32.63
Lira	2.13	33.38
Nimule	3.63	32.13

Source: http://iridl.ldeo.columbia.edu/SOURCES/.NASA/.GES-DAAC/.TRMM_L3/.TRMM_3B42/.v7/%20.daily/ (with a resolution of 0.25° by 0.25° or 32 by 32 Km).

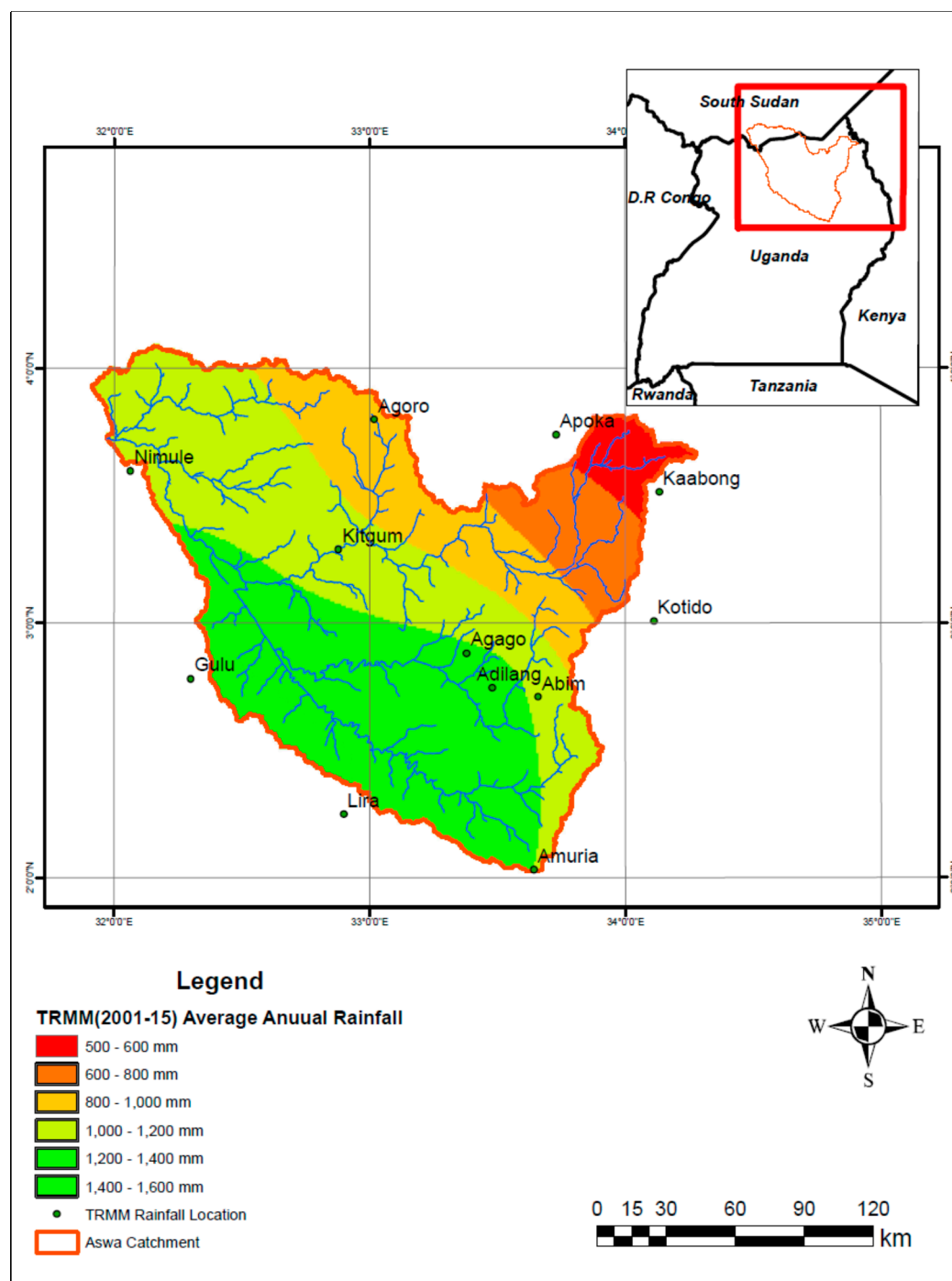


Figure 1. Location of Aswa River catchment and GIS generated average Tropical Rainfall Measuring Mission (TRMM) annual rainfall (2000–2015) distribution.

2.2. Rainfall Data

Secondary data from TRMM rainfall were used for this study in place of the scarce and inconsistent recorded rainfall data over the catchment. Gridded satellite based TRMM data are available from 2000 to 2015 (16 years). The TRMM rainfall data grid locations used in this study are shown in Table 1. The TRMM grid resolution is 32 by 32 Km, while for the GCM used is within 290 by 435 km. The TRMM data can therefore be used for downscaling GCM data to a finer resolution.

2.3. Data Processing

Limited observed daily rainfall data are available within the vicinity of the Aswa catchment from weather stations such as Lira, Gulu and Kitgum. The relation between the station and secondary data (TRMM) was investigated through correlation to find out if they were closely related enough to give confidence of using TRMM data in calibrating the statistical downscaling model over the catchment. Sometimes secondary data may have interventions due to malfunction of satellite equipment or change of equipment [27] and, therefore, should be tested before use so that the homogenous section is used for the study. Before this validation, TRMM data were put to intervention test analysis to find out if the data set was homogeneous using the standard normal homogeneity test (SNHT) [15].

2.4. Downscaling and Projection of Future Rainfall

TRMM rainfall data were used to calibrate the SDSM for subsequent downscaling of two GCMs (HadCM3 and CanESM2). Many GCMs are in use today, globally, with varying degrees of accuracy. CanESM2 and HadCM3 have been successfully used in the region for climate change studies [28,29] and have, therefore, been adopted for use in this study. The high emission scenario RPC 8.5 (CanESM2), A2 (HadCM3) predictor data variables were used for this study to represent the worst-case scenario. The predictor data for the two GCMs were obtained from two different websites: HadCM3 (<http://www.cccsn.ec.gc.ca/?page=pred-hadcm3>) and CanESM2 (<http://www.cccsn.ec.gc.ca/?page=pred-canesm2>).

The predictor variables were screened in order to choose appropriate predictors. This stage is critical because the choice of predictors largely determines the accuracy of the downscaled climate scenario data. The procedure for predictor selection has been well laid by Hasan, et al. [30]. A correlation matrix between the predictor and predictand (TRMM rainfall) was made. The predictor with the highest correlation coefficient was selected and called the super predictor (SP). After choosing the super predictor, the remaining predictors were regressed individually, together with SP, and the absolute correlation coefficient between the predictor and predictand and between individual predictors were obtained together, with their partial correlations and P values. Any predictor with p -value $> \alpha$ (0.05) was removed. The percentage by which partial correlation is lowered in respect to the correlation coefficient PRP (Equation (1)) was calculated for each predictor. The other predictors were selected by calculating the PRP with respect to the absolute correlation using the following equation.

$$PRP = \left(\frac{P.r - R1}{R1} \right) \quad (1)$$

where:

PRP is the percentage by which partial correlation is lowered in respect to the correlation coefficient, $P.r$ is defined as partial correlation coefficient and

$R1$ is the value of correlation coefficient between predictor and predictand.

The predictor that had the minimum PRP was selected as the second most suitable predictor. This same process was done for the third and other following predictors. As a result, the super predictor and the other remaining predictors will have almost zero, or insignificant multi-co-linearity. Five predictors were selected, as can be seen, for example, for the Kitgum location in Table 2, with mean temperature at 2 m as the super predictor. The correlations are statistically significant ($p < 0.05$).

Table 2. Predictor selection for Kitgum Rainfall.

Predictor Description	R1	P.r	P	PRP = ((P.r – R1)/R1)	P.r	P	PRP = ((P.r – R1)/R1)	P.r	P	PRP = ((P.r – R1)/R1)	P.r	P	PRP = ((P.r – R1)/R1)	Rank
Mean temperature at 2 m	0.59													Super Predictor
Surface specific humidity	0.54	0.29	0.00	0.46	0.19	0.00	0.64	0.07	0.00	0.87	0.03	0.07	0.94	
850 hPa zonal velocity	0.52	0.37	0.00	0.29										2nd
Specific humidity at 850 hPa	0.50	0.31	0.00	0.39	0.22	0.00	0.55							3rd
Surface zonal velocity	0.49	0.32	0.00	0.36	0.10	0.00	0.79	0.12	0.00	0.76	0.10	0.00	0.79	
850 hPa airflow strength	0.45	0.31	0.00	0.30	0.07	0.00	0.84	0.09	0.00	0.79	0.08	0.00	0.83	
Surface airflow strength	0.44	0.26	0.00	0.40	0.09	0.00	0.80	0.11	0.00	0.76	0.09	0.00	0.79	
Specific humidity at 500 hPa	0.43	0.24	0.00	0.44	0.19	0.00	0.55	0.10	0.00	0.76	0.12	0.00	0.74	5th
precipitation	0.37	0.17	0.00	0.53	0.04	0.01	0.89	0.10	0.00	0.72				4th

Key: PRP is the percentage by which partial correlation is lowered in respect to the correlation coefficient, P.r is partial correlation coefficient, R1 is the value of correlation coefficient between predictor and predictand, P is probability value. Values in bold indicate the highest correlation coefficient for R1 column or the lowest PRP value in the PRP column.

Calibration and Validation of SDSM Model and Generation of Future Rainfall

SDSM version 4.2.9 was calibrated and validated using the selected appropriate predictors and TRMM rainfall data as predictand for various locations within the Aswa catchment. Such results of predictor selection are shown for Kitgum station in Table 2.

Using the developed model, precipitation data were simulated for 1961–2001 (HadCM3) and 1961–2005 (CanESM2). The SDSM was used to generate 20 ensembles. The mean of the ensembles and the TRMM and SDSM weather generator monthly rainfall data were compared. The coefficient of determination, R^2 , between the (TRMM) and generated monthly data series, Bias (ratio of sum of totals of simulated and TRMM rainfall), F values and the standard error (SE), were used for evaluation of the statistical calibration and validation. The calibration and validation results for various locations within the catchment can be seen in Table 3. The results show that the statistical calibration and validation are good enough to be relied on. The correlation coefficients range from 0.83 to 0.97. The analysis of variance (ANOVA) F values are much greater than the critical values and the standard error for rainfall range from 9.62 to 29.25 mm/month. These values compare well with other studies using SDSM and validation studies in the region [28,29,31]. The bias values are low, with an average value of 1.018.

Table 3. Calibration and validation of Statistical down Scaling Model (SDSM) results for various locations within the Aswa catchment.

Location	GCM	Parameter	Process	Bias	Regression Statistics			ANOVA		
					R	R ²	Standard Error	Observations	F	Significance of F
Agago	HadCM3	Rainfall	Calibration	Period	1975–1990(16yrs)	1.034	0.87	0.76	29.25	192
			Validation							
	CanESM2	Rainfall	Calibration		1991–2001(11yrs)	0.988	0.88	0.77	26.93	132
			Validation							
Agoro	HadCM3	Rainfall	Calibration	Period	1975–1990(16yrs)	1.021	0.97	0.95	13.84	192
			Validation							
	CanESM2	Rainfall	Calibration		1991–2005(15yrs)	1.010	0.97	0.95	12.64	180
			Validation							
Amuria	HadCM3	Rainfall	Calibration	Period	1975–1990(16yrs)	1.048	0.85	0.72	21.03	192
			Validation							
	CanESM2	Rainfall	Calibration		1991–2001(11yrs)	0.996	0.93	0.86	14.11	132
			Validation							
Kaabong	HadCM3	Rainfall	Calibration	Period	1975–1990(16yrs)	0.964	0.95	0.90	12.33	192
			Validation							
	CanESM2	Rainfall	Calibration		1991–2005(15yrs)	1.011	0.91	0.83	15.43	180
			Validation							
Gulu	HadCM3	Rainfall	Calibration	Period	1975–1990(16yrs)	1.030	0.87	0.76	26.82	192
			Validation							
	CanESM2	Rainfall	Calibration		1991–2001(11yrs)	1.055	0.86	0.74	26.43	132
			Validation							
Gulu	HadCM3	Rainfall	Calibration	Period	1975–1990(16yrs)	1.044	0.94	0.88	19.36	192
			Validation							
	CanESM2	Rainfall	Calibration		1991–2005(15yrs)	1.057	0.95	0.90	16.15	180
			Validation							
Gulu	HadCM3	Rainfall	Calibration	Period	1975–1990(16yrs)	0.995	0.90	0.81	15.44	192
			Validation							
	CanESM2	Rainfall	Calibration		1991–2001(11yrs)	1.136	0.83	0.69	15.75	132
			Validation							
Gulu	HadCM3	Rainfall	Calibration	Period	1975–1990(16yrs)	0.980	0.95	0.89	11.59	192
			Validation							
	CanESM2	Rainfall	Calibration		1991–2005(15yrs)	0.966	0.94	0.89	9.62	180
			Validation							
Gulu	HadCM3	Rainfall	Calibration	Period	1975–1990(16yrs)	1.019	0.96	0.92	19.19	192
			Validation							
	CanESM2	Rainfall	Calibration		1991–2001(11yrs)	0.982	0.93	0.87	23.21	132
			Validation							
Gulu	HadCM3	Rainfall	Calibration	Period	1975–1990(16yrs)	1.019	0.97	0.95	15.45	192
			Validation							
	CanESM2	Rainfall	Calibration		1991–2005(16yrs)	0.998	0.96	0.92	18.18	180
			Validation							

The calibrated SDSM was used to downscale HadCM3 and CanESM2 for a generation of future rainfall data for the near future (2006–2035), medium term future (2036–2065) and long term future (2066–2099). These data were analyzed for trends and variability following the procedure outlined in Section 2.5.

2.5. Rainfall Trend Analysis

The historical (secondary) TRMM (2000–2015) data were subjected to a homogeneity test in order to identify any interventions in the data. The homogenous portion of the data was then used for further analysis. The simulated near future (2006–2035), medium term (2036–2065) and the long term (2066–2099) future daily and monthly rainfall data were analyzed for trend and variability. The Mann–Kendall test was used for trend analysis and is given by Equations (2) and (3).

$$\tau = \frac{S}{0.5 * n * (n - 1)} \quad (2)$$

$$S = \sum_{i=1}^{n-1} \sum_{j=i+1}^n \text{sign} (x_j - x_i) \quad (3)$$

where;

x_j = the observation at time j

x_i = the observation at time i

n = total number of observations

Sign ($x_j - x_i$) = 1 if computed value > 0
 = 0 if computed value is 0
 = −1 if computed value < 0

Further analysis was carried out using descriptive statistics such as mean, standard error, standard deviation and coefficient of variability (CV) for the historical (TRMM) and simulated future rainfall data.

2.6. Onset and Cessation of Rainfall Dates

The cumulative percentage mean rainfall method was used to determine the onset and cessation of the historical, near future (2006–35), medium term (2036–65) and long term (2066–99) future simulated rainfall. This method has been used successfully by many researchers [7,32–34] for determination of the rainfall onset and cessation dates. The procedure for the method is as follows:

1. the percentage of mean annual rainfall that happens at every 5-day interval is derived;
2. the cumulative percentage of the computed percentage at 5-day intervals is derived;
3. the cumulative percentage at 5-day intervals is plotted for the whole year; and
4. identification of the time of rainfall onset and cessation during the year or season.

The point of first maximum positive curvature and last maximum negative curvature on the graph of the cumulative percentage indicate the mean periods of rainfall onset and cessation, respectively. Another alternative criterion for the onset of the rain is the timing of an accumulated 7% to 8% of the annual rainfall, and the cessation begins after the accumulation of 90% of the annual rainfall.

The cumulative percentage mean rainfall method for determining onset and cessation of rainfall can use either the rainfall amounts or rainy days [7,32,33,35]. Both methods have been applied in this study. There are other methods for determination and definitions of onset and cessation of rain [36,37]. The criterion used for defining onset and cessation of rain can be based on soil water balance/water stress coefficient, the first wet day with accumulated X mm of rainfall during a period of a certain number of days, rainfall–evapotranspiration relation model, and others. The threshold for a rainy day also varies: 0.85 mm, 1 mm and other values [36,38]. The method of cumulative percentage mean rainfall is commonly used by many researchers. It is preferred to other methods for determination of rainfall onset and cessation dates due to its efficiency and freedom from assumption of rainfall threshold values and its reliance on rainfall data alone [39]. The minimum rainfall value for a rainy day was set as 1 mm. This value was adopted from Ngetich, Mucheru-Muna, Mugwe, Shisanya, Diels and Mugendi [36]. The days with rainfall below 1 mm were considered as non-rainy or dry days.

2.7. Standardized Precipitation Index (SPI)

There are several drought indices in use but the most commonly used are the Palmer Drought Severity Index (PDSI) and the Standardized Precipitation Index (SPI) [40,41]. The PDSI is related to a water balance. The input parameters include moisture supply, evaporation, precipitation and runoff. However, the SPI is an index with only precipitation as an input variable [42]. The standardized Precipitation Index (SPI) was used to determine occurrence of extreme rainfall events for the current period and future projections of rainfall in this study. The advantage of SPI over other indices is its robustness to detect different types of droughts such as hydrological, meteorological and agricultural at different time scales (1, 3, 6, 12, 24 up to 60 months) using only rainfall data set.

The SPI computation method was developed by McKee, et al. [43] to evaluate the relative deviations of precipitation from the average normal values and the Gamma distribution is generally used in SPI calculation. It has been used for many studies all over the world [41,44–48] to evaluate occurrences or drought and wet conditions. SPI is based on normalized data and, therefore, does not vary spatially, and as such, droughts and wet occurrences can be assessed in different regions. The SPI is calculated by fitting a certain probability density function to the frequency distribution of rainfall series over the period for the analysis. The resulting fitted function is used to generate cumulative distribution of the data and consequently transformed into the standardized normal distribution used to define SPI.

The Gamma distribution has two main parameters; the probability density function (PDF) and cumulative distribution function (CDF).

The PDF can be expressed as:

$$g(X) = \frac{1}{\beta^\alpha \Gamma^\alpha} x^{\alpha-1} e^{-x/\beta} \quad (4)$$

where,

α = shape parameter ($\alpha > 0$),

β = scale parameter ($\beta > 0$),

Γ^α = a gamma function of α and can be expressed as;

$$\Gamma(\alpha) = \int_0^\infty y^{\alpha-1} e^{-y} dy \quad (5)$$

The PDF of an observed amount of precipitation for a given month and period of time is expressed as:

$$G(x) = \frac{1}{\hat{\beta}^\alpha \Gamma(\hat{\alpha})} \int_0^x x^{\alpha-1} e^{-x/\hat{\beta}} dx \quad (6)$$

The PDF is transformed to the standard normal variate Z , which is the value of SPI.

$$SPI = \frac{x_i - \bar{x}}{\sigma} \quad (7)$$

where, x_i is the precipitation of the selected period during the year i , \bar{x} is the long term mean precipitation and σ is standard deviation for the selected period. Positive and negative SPI values correspond to wet and drought periods respectively. Table 4 gives the classification of SPI values.

Table 4. Classification of SPI values.

SPI Value	Class
2.00 or more	Extremely wet
1.50–1.99	Severely wet
1.00–1.49	Moderately wet
0–0.99	Mildly wet
0 to −0.99	Mildly dry
−1.00 to −1.49	Moderately dry
−1.50 to −1.99	Severely dry
−2 or less	Extremely dry

Source: [44].

In this study, hydrological drought was evaluated for Aswa catchment. A soft wear SPI generator developed by the National Drought Mitigation Center of University of Nebraska-Lincoln was used to calculate the monthly SPI values for the period 2006–2099.

3. Results

3.1. Correlation of Station and TRMM Rainfall

The TRMM and Observed monthly rainfall data for Lira station were correlated as seen in (Figure 2). The correlation gives coefficient of determination, R^2 value of 0.65 and standard error of 47.86 mm. This indicates that the observed and TRMM rainfall data are closely correlated and the TRMM data can be used to represent observed data in case of unavailability of the latter.

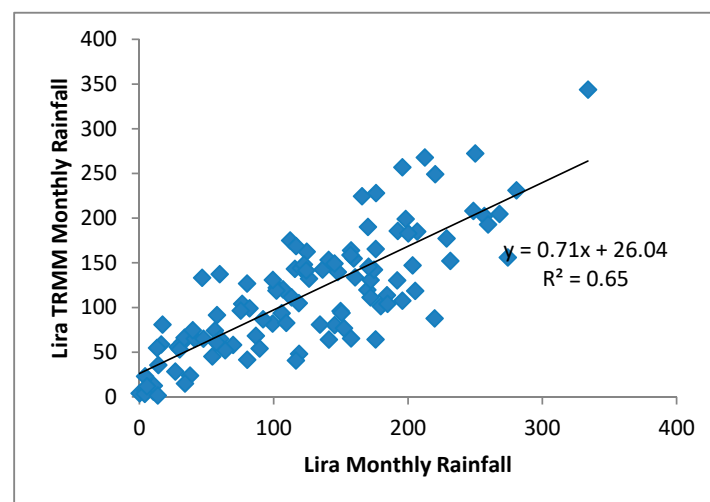
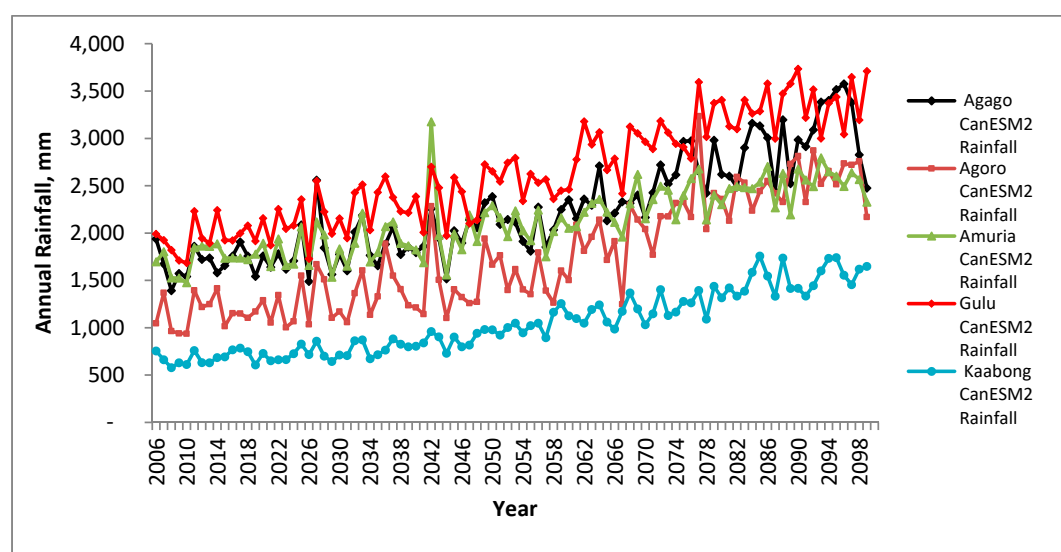


Figure 2. Correlation of TRMM and observed rainfall data for Lira.

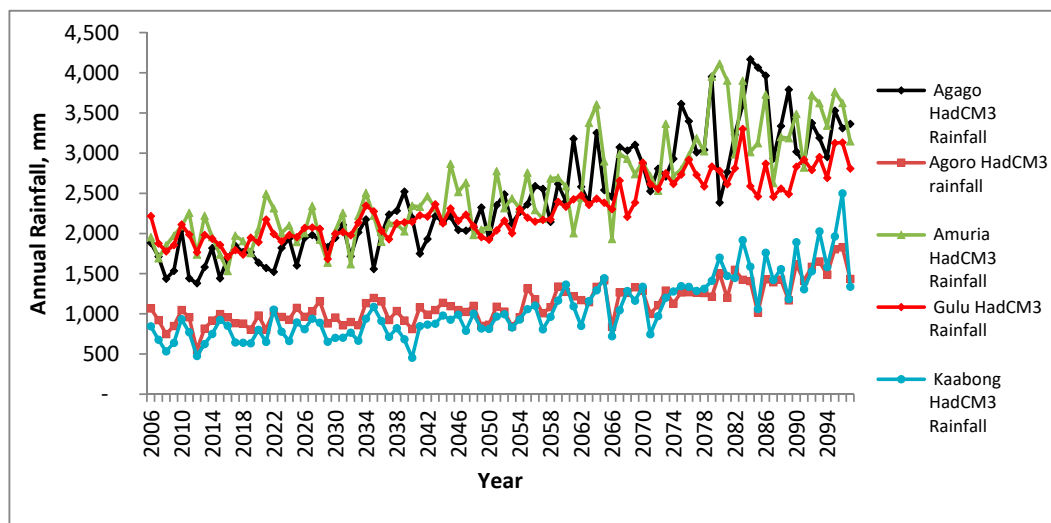
3.2. Simulated Future Rainfall

Based on computed test statistics against threshold, homogeneity test results (Table 5) show that the TRMM and weather generated rainfall data series 1975–2005 are homogeneous and, therefore, the whole data series was used to calibrate the SDSM for the study. Future rainfall scenarios were subsequently simulated using the calibrated and validated SDSM for two GCMs (HadCM3 and CanESM2) for various locations within the vicinity of the Aswa catchment. All of the results show future rise in rainfall amounts. Figure 3 shows the graphical simulation results for five locations based on CanESM2 and HadCM3 GCMs.



(a)

Figure 3. Cont.



(b)

Figure 3. Simulated future rainfall for Agago, Amuria, Gulu, Agoro and Kaabong locations (a) CanESM2-SDSM (2006–2100) (b) HadCM3-SDSM (2006–2097).

The annual rainfall at current (2015) level for Agoro is about 800 mm and is expected to rise to about 1000–1200 mm by 2035, 1200–1300 mm by 2065 and up to 1500 mm by 2099 (Figure 3). The annual rainfall at current level for Amuria is about 1500 mm and is expected to rise to about 1700–2000 mm by 2035, 2200–2300 mm by 2065 and up to 3500 mm by 2099 (Figure 3).

The Mann–Kendall test statistics also show that there is going to be positive trend for the simulated future annual rainfall over Aswa catchment as can be seen from Table 5. The Kendall tau values range from 0.172 to 0.683. The increase in positive trend is steeper for the medium term (2036–2065) and long term (2066–2099) periods. This increase in rainfall is also associated with increased variability as we show in the next sections.

The increase in annual rainfall is expected to have impact on agricultural production, water resources and environment management. Some of the impacts may be positive (increased crop yields, water availability) while others may be negative (erosion, flooding, infrastructure damage, increased waterborne diseases).

Table 5. Results of Homogeneity Test and Mann–Kendall Statistics for TRMM and Simulated Rainfall Data for Agoro and Amuria Locations in Aswa Catchment. SNHT = standard normal homogeneity test.

GCM, Location	Data Type	Period	Homogeneity Test-SNHT			Number of Observations	Mann–Kendall Statistics		
			<i>p</i> -Value (Two-Tailed)	Alpha	Comment		Kendall's Tau	Sen's Slope	Comment
CanESM2									
Agoro	TRMM and generated monthly Rainfall	1975–2005	0.099	0.05	$p > \alpha$ (0.05), homogeneous	372			
	TRMM and simulated annual Rainfall	2006–2099				94	0.683	18.52	Positive trend
	TRMM and simulated annual Rainfall	2006–2065				60	0.449	10.42	Positive trend
	TRMM and simulated annual Rainfall	2006–2035				30	0.200	6.628	Positive trend
HadCM3									
Agoro	TRMM and simulated annual Rainfall	2006–2097				92	0.669	3.219	Positive trend
	TRMM and simulated annual Rainfall	2006–2065				60	0.463	2.339	Positive trend
	TRMM and simulated annual Rainfall	2006–2035				30	0.195	1.426	Positive trend
CanESM2									
Amuria	TRMM and generated monthly Rainfall	1975–2005	0.220	0.05	$p > \alpha$ (0.05), homogeneous	372			
	TRMM and simulated annual Rainfall	2006–2100				94	0.647	10.52	Positive trend
	TRMM and simulated annual Rainfall	2006–2065				60	0.472	9.072	Positive trend
	TRMM and simulated annual Rainfall	2006–2035				30	0.172	6.286	Positive trend
HadCM3									
Amuria	TRMM and simulated annual Rainfall	2001–2097				92	0.647	18.54	Positive trend
	TRMM and simulated annual Rainfall	2001–2065				60	0.482	13.70	Positive trend
	TRMM and simulated annual Rainfall	2001–2035				30	0.218	9.212	Positive trend

3.3. Future Rainfall Onset and Cessation Dates

The onset and cessation of rainfall is to vary in the future and depart from the present pattern. In the mid and long term future, onset of rain is expected earlier by 3–4 weeks and rainfall cessation is expected to also commence later than it occurs now, by 1–5 weeks. The rainfall cessation dates are more variable than the onset dates. Figures 4–11 show examples of the mean rainfall onset and cessation dates for present, near, medium and long term future simulations for Agago and Kaabong locations using daily rainfall and rainy days data. These two locations can be seen from Figure 1. Kaabong represents the semi-arid part of the catchment and Agago the humid part. Results for both CanESM2 and HadCM3 predictions are comparably close to each other. However, the future rainfall onset and cessation dates are to become more variable. Some studies from Ghana [32] found that the use of daily rainfall or rainy days for determination of onset and cessation of rainfall give similar results. Odekunle [33] showed that the use of rainy days for determination of onset and cessation of rainfall in Nigeria gave more accurate results than the use of rainfall amounts. However, in our work for Aswa catchment, there is no evidence that this is the case as the two methods gave similar results.

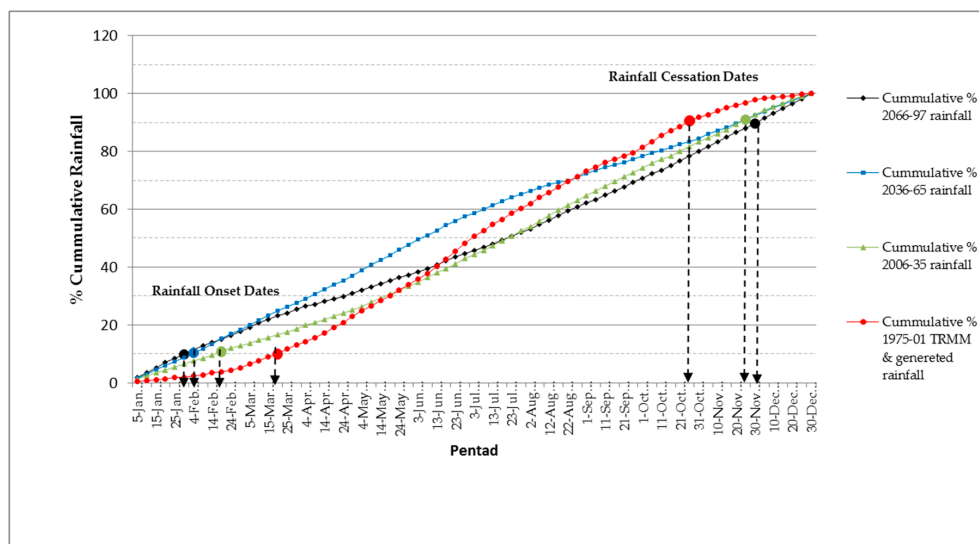


Figure 4. Agago Future Mean Rainfall Onset and Cessation (TRMM, weather generated Rainfall (1975–2001) and projected (HadCM3) 2006–2035, 2006–2065 and 2006–2099).

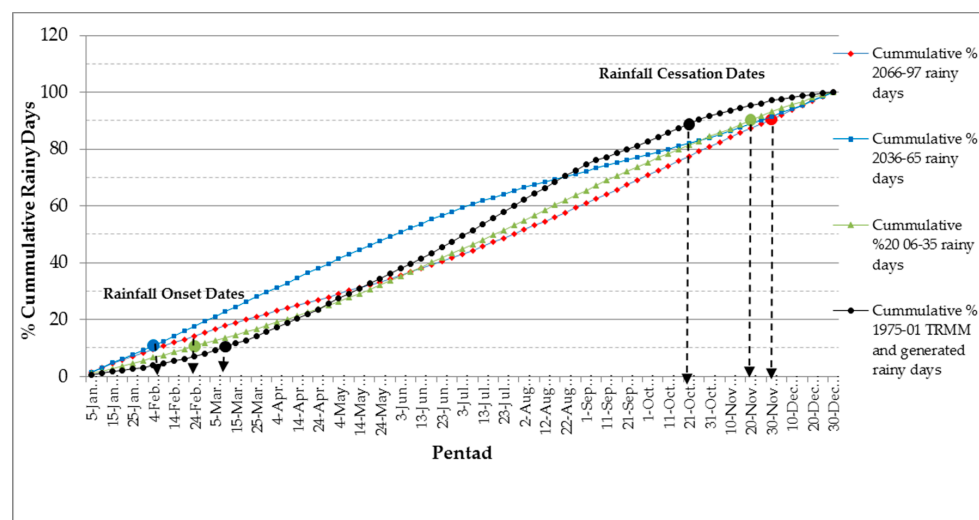


Figure 5. Agago Future Mean Rainfall Onset and Cessation for Rainy Days (TRMM Rainfall (1975–2001) and projected (HadCM3) 2006–2035, 2006–2065 and 2006–2099).

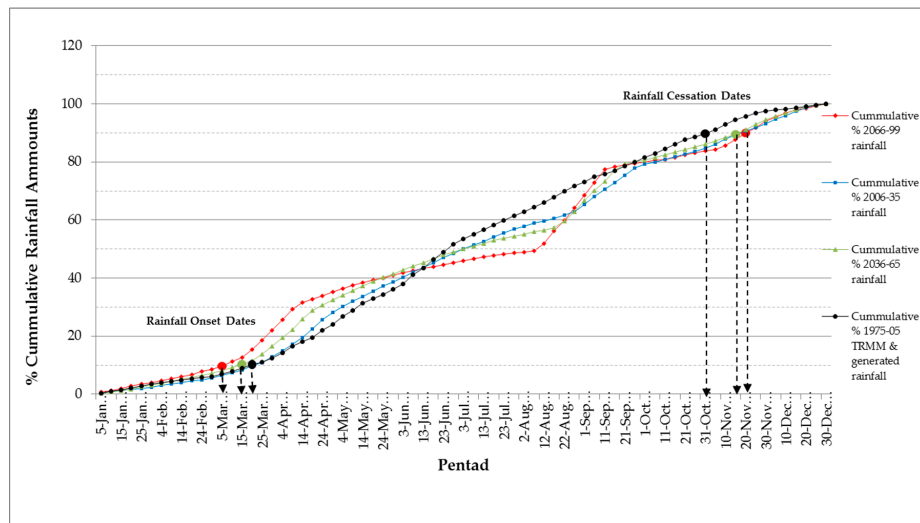


Figure 6. Agago Future Mean Rainfall Onset and Cessation (TRMM Rainfall (1975–2005) and projected (CanESM2) 2006–2035, 2036–2065 and 2066–2099).

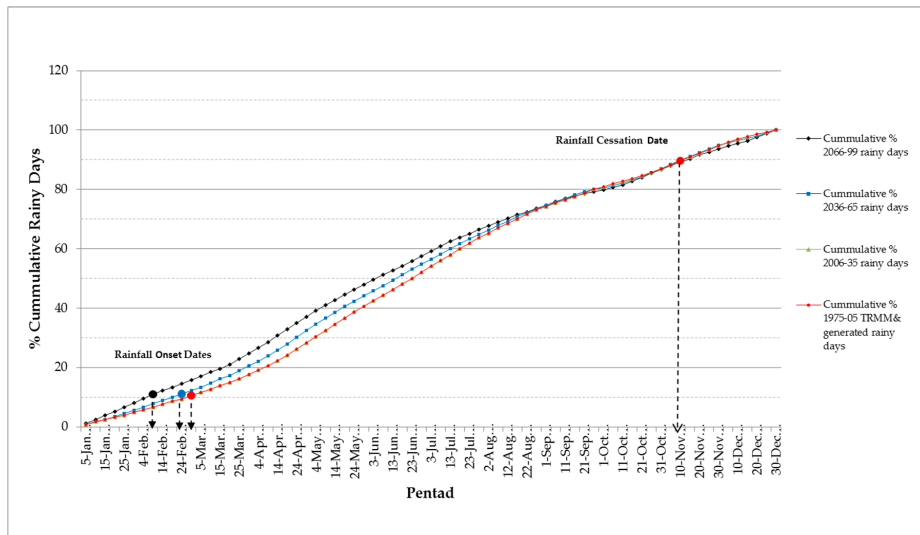


Figure 7. Agago Future Mean Rainfall Onset and Cessation for Rainy Days (TRMM Rainfall (1975–2005) and projected (CanESM2) 2006–2035, 2036–2065 and 2066–2099).

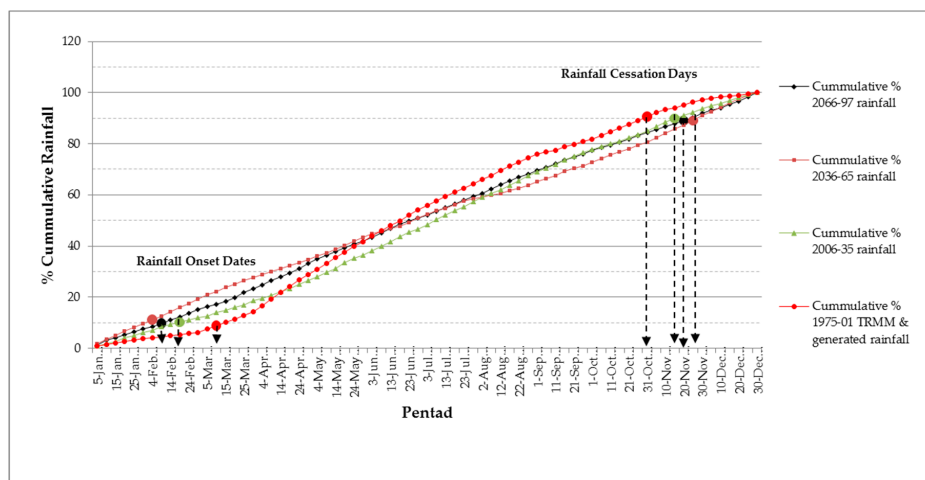


Figure 8. Kaabong Future Mean Rainfall Onset and Cessation Dates (TRMM rainfall (1975–2001) and projected (HadCM3) 2006–2035, 2036–2065 and 2066–2099).

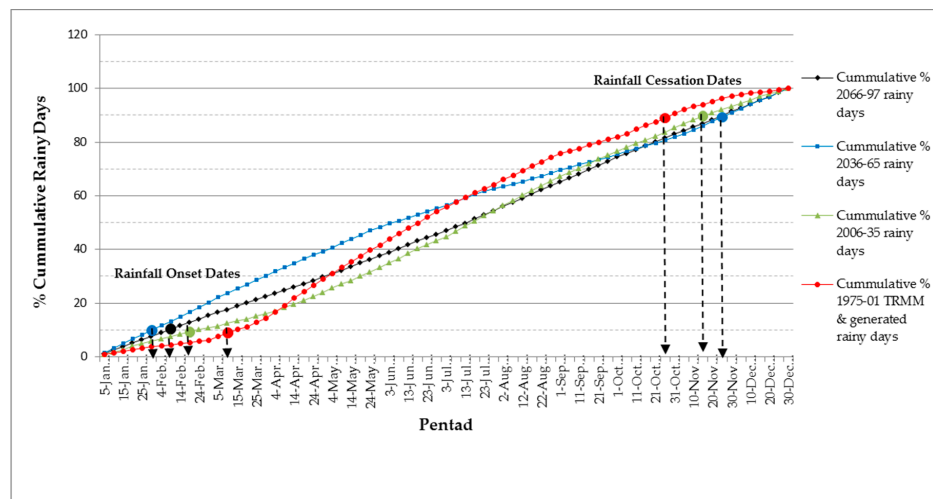


Figure 9. Kaabong Future Mean Rainfall Onset and Cessation for Rainy Days (TRMM rainfall (1975–2001) and projected (HadCM3) 2006–2035, 2036–2065 and 2066–2099).

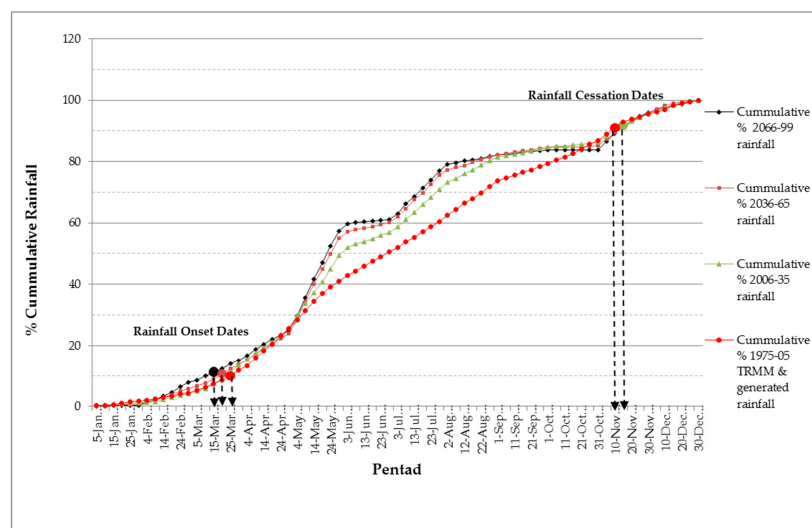


Figure 10. Kaabong Future Mean Rainfall Onset and Cessation Dates (TRMM rainfall (1975–2005) and projected (CanESM2) 2006–2035, 2036–2065 and 2066–2099).

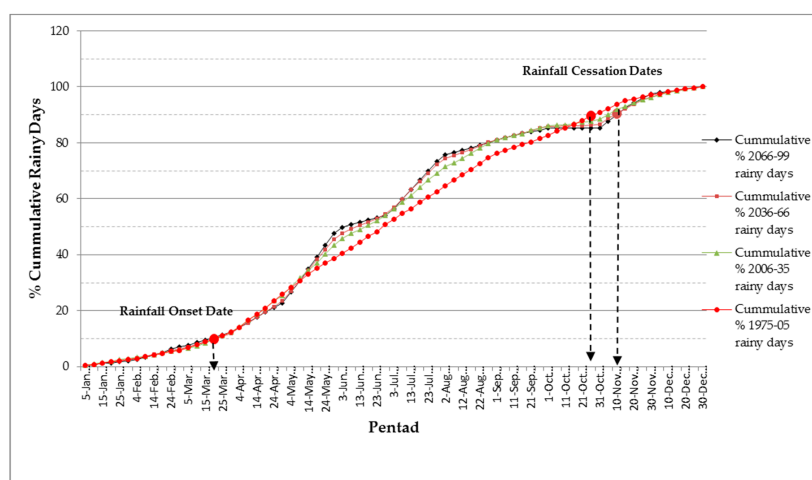


Figure 11. Kaabong Future Mean Rainfall Onset and Cessation for Rainy Days (TRMM rainfall (1975–2005) and projected (CanESM2) 2006–2035, 2036–2065 and 2066–2099).

In view of the observations above, it is expected that the future shift of the onset and cessation of rainfall will have impact on the planning and management of farming activities in Aswa catchment. It will also impact crops yields in the catchment. Introduction of new crop varieties, which have short growing periods, irrigation, soil and water conservation may be some of the mitigation measures to be adopted by farmers in the catchment.

3.4. Rainfall Variability Analysis

The simulated future rainfall data series are highly variable. The monthly coefficients of Variation (CV) reach up to 118.5%. Coefficient of variation is a measure of how reliable the rainfall pattern is. A higher variability implies a highly unreliable rainfall pattern. Generally, rainfall with a CV value above 30% is considered to be highly variable [49]. Tables 6–8 summarize the results for Agoro, Kaabong and Gulu locations, respectively. Kaabong represents the semi-arid region, Agoro represents the semi-humid region and Gulu represents the humid region of the catchment, as can be seen in Figure 1.

Table 6. Agoro TRMM and Simulated (CanESM2 and Had3) Monthly Rainfall Coefficient of Variation.

	Jan.	Feb.	Mar.	Apr.	May	Jun.	Jul.	Aug.	Sep.	Oct.	Nov.	Dec.
CanESM2												
1975–2005 TRMM and Weather Generator												
Mean	24.2	28.4	48.2	116.9	74.1	83.2	108.9	117.3	55.9	83.8	65.9	25.0
Standard Deviation	18.4	23.0	10.6	24.1	18.8	13.7	11.1	23.6	13.4	15.5	28.1	10.0
CV, %	76.1	80.8	22.0	20.6	25.3	16.5	10.2	20.1	24.0	18.5	42.7	40.1
2006–2035 TRMM and Simulation												
Mean	21.5	58.0	84.0	164.2	123.6	79.9	56.2	191.4	159.4	56.6	166.3	52.9
Standard Deviation	7.2	55.8	38.6	52.9	37.4	23.8	16.4	30.0	51.8	27.8	92.7	20.6
CV	33.4	96.3	46.0	32.2	30.3	29.7	29.1	15.7	32.5	49.0	55.7	38.9
2006–2065 TRMM and Simulation												
Mean	24.2	96.6	107.2	209.9	145.8	97.2	47.7	195.1	197.9	58.1	160.8	49.8
Standard Deviation	8.3	110.3	72.5	80.6	40.2	36.1	15.7	33.3	74.0	68.8	91.2	18.5
CV	34.4	114.1	67.7	38.4	27.6	37.1	32.8	17.1	37.4	118.5	56.7	37.1
2006–2099 TRMM and Simulation												
Mean	28.7	224.0	150.0	246.5	176.3	128.8	40.4	206.1	271.7	54.4	171.0	47.9
Standard Deviation	14.2	255.4	94.9	103.5	59.9	60.9	16.6	34.5	126.7	62.1	101.5	16.6
CV, %	49.4	114.0	63.3	42.0	34.0	47.3	41.1	16.7	46.6	114.0	59.4	34.7
HadCM3												
1975–2001 TRMM and Weather Generator												
Mean	46.6	38.6	49.1	62.7	74.1	73.6	101.8	101.0	92.9	86.3	74.7	55.8
Standard Deviation	26.5	21.5	32.0	44.8	42.4	30.3	34.7	26.6	28.2	23.8	35.3	33.0
CV, %	56.9	55.7	65.1	71.3	57.2	41.1	34.0	26.3	30.3	27.6	47.2	59.1
2006–2035 TRMM and Simulation												
Mean	46.6	38.6	49.1	62.7	74.1	73.6	101.8	101.0	92.9	86.3	74.7	55.8
Standard Deviation	26.5	21.5	32.0	44.8	42.4	30.3	34.7	26.6	28.2	23.8	35.3	33.0
CV, %	56.9	55.7	65.1	71.3	57.2	41.1	34.0	26.3	30.3	27.6	47.2	59.1
2006–2065 TRMM and Simulation												
Mean	66.9	73.7	83.7	83.8	89.2	76.9	78.9	69.6	61.9	67.3	72.0	67.7
Standard Deviation	39.7	53.3	54.4	49.0	45.6	41.8	44.3	42.9	40.9	42.4	45.3	40.0
CV, %	59.4	72.3	65.0	58.5	51.1	54.4	56.1	61.6	66.0	63.0	62.9	59.2
2006–2097 TRMM and Simulation												
Mean	77.7	67.2	67.4	65.6	76.3	74.6	80.5	85.4	89.5	89.8	90.4	83.6
Standard Deviation	57.9	52.7	53.6	50.7	52.0	47.2	46.0	57.1	66.3	61.5	64.7	55.3
CV, %	74.5	78.4	79.5	77.3	68.1	63.3	57.1	66.9	74.1	68.5	71.6	66.1

The red and black items show the high CV values. The red color gives the highest CV values for rainfall onset and cessation periods.

Table 7. Kaabong TRMM and Simulated (CanESM2 and HadCM3) Monthly Rainfall Coefficient of Variation.

	<i>Jan.</i>	<i>Feb.</i>	<i>Mar.</i>	<i>Apr.</i>	<i>May</i>	<i>Jun.</i>	<i>Jul.</i>	<i>Aug.</i>	<i>Sep.</i>	<i>Oct.</i>	<i>Nov.</i>	<i>Dec.</i>
CanESM2												
1975–2005 TRMM and Weather Generator												
Mean	9.9	12.4	47.5	76.2	90.4	51.5	63.9	67.0	28.8	40.5	43.9	24.4
Standard Deviation	6.4	4.6	16.1	15.5	35.5	14.0	7.5	19.6	9.5	13.7	17.6	16.4
CV, %	65.1	36.8	33.8	20.3	39.3	27.1	11.8	29.3	33.0	33.7	40.1	67.5
2006–2035 TRMM and Simulation												
Mean	7.3	21.0	70.3	92.8	172.8	41.7	111.1	61.6	24.8	12.2	58.1	34.2
Standard Deviation	1.2	9.6	23.5	18.5	41.8	11.7	23.1	19.6	5.5	6.6	15.5	15.9
CV, %	16.2	45.7	33.4	20.0	24.2	28.2	20.8	31.8	22.2	54.1	26.7	46.5
2006–2065 TRMM and Simulation												
Mean	7.3	37.2	77.7	101.0	239.2	39.2	133.5	55.1	24.2	8.3	76.3	38.0
Standard Deviation	1.2	26.1	32.3	24.0	87.8	10.9	35.0	18.8	5.1	6.7	32.1	17.7
CV, %	15.7	70.1	41.6	23.7	36.7	27.9	26.2	34.1	21.0	81.2	42.1	46.5
2006–2099 TRMM and Simulation												
Mean	7.2	64.5	91.2	114.1	322.5	34.5	172.8	51.6	23.6	5.8	107.7	43.2
Standard Deviation	1.8	48.3	38.5	31.8	139.1	12.1	66.3	18.2	5.1	6.5	67.5	21.2
CV, %	25.2	74.9	42.3	27.8	43.1	35.1	38.4	35.3	21.6	111.8	62.6	49.1
HadCM3												
1975–2001 TRMM and Weather Generator												
Mean	11.2	14.6	68.7	85.3	102.6	56.0	52.1	66.4	25.4	51.1	62.8	27.5
Standard Deviation	3.7	4.3	20.0	9.1	30.5	10.2	5.3	5.4	3.0	6.7	12.6	12.3
CV, %	32.9	29.2	29.2	10.6	29.7	18.3	10.3	8.1	11.8	13.2	20.0	44.8
2006–2035 TRMM and Simulation												
Mean	49.1	51.2	66.0	77.1	87.6	90.7	102.6	96.4	80.4	74.5	73.9	62.4
Standard Deviation	25.8	39.0	48.6	62.0	60.4	40.3	34.3	41.5	32.4	30.3	23.5	32.8
CV, %	52.5	76.2	73.7	80.4	69.0	44.4	33.5	43.1	40.4	40.6	31.8	52.6
2006–2065 TRMM and Simulation												
Mean	88.4	86.6	93.9	88.3	103.1	101.0	97.8	92.2	94.2	95.2	100.9	97.8
Standard Deviation	58.2	58.4	53.9	52.1	63.1	38.5	35.8	46.0	75.7	71.9	69.1	72.2
CV, %	65.9	67.5	57.4	59.0	61.3	38.1	36.6	49.9	80.3	75.6	68.5	73.8
2006–2097 TRMM and Simulation												
Mean	120.8	109.8	127.7	127.5	135.1	135.8	130.1	128.3	120.0	117.3	123.6	132.8
Standard Deviation	79.1	78.7	100.2	109.6	96.3	115.7	83.7	81.0	80.6	75.3	87.6	89.9
CV, %	65.5	71.7	78.5	86.0	71.3	85.2	64.3	63.1	67.2	64.2	70.8	67.7

The red and black items show the high CV values. The red color gives the highest CV values for rainfall onset and cessation periods.

As suggested by the high CV values, the rainfall is expected to be more variable during the onset and cessation months of February–April and September–November, respectively. There is a short dry spell that occurs around the months of June–July. The rainfall projection based on CanESM2 show that the short dry spell of July is to be more severe in the mid and long term future than the current period as shown in Figures 12 and 13 for Agoro and Gulu locations. Extreme heavy rainfall events are expected to increase during February–May, September and November months.

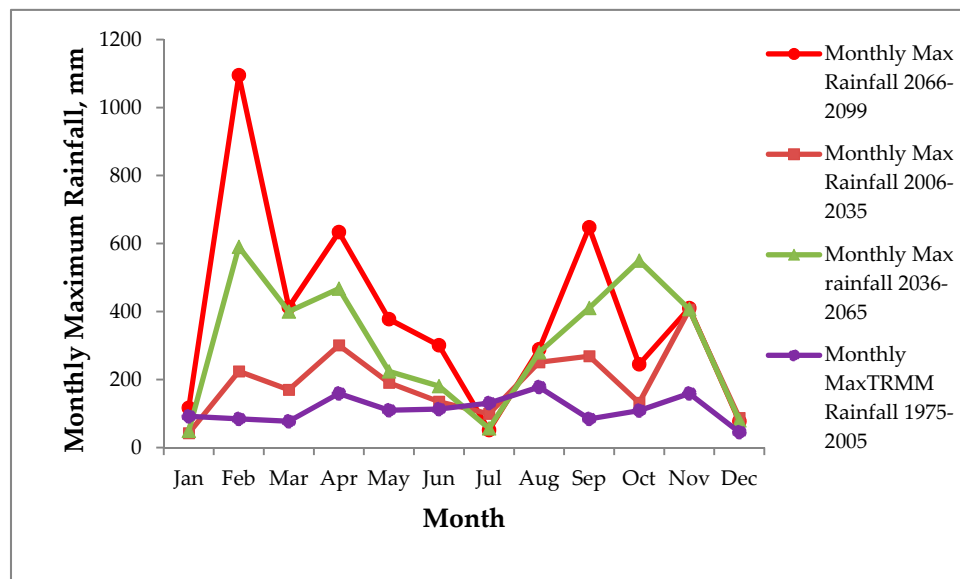
Table 8. Gulu TRMM and Simulated (CanESM2 and HadCM3) Monthly Rainfall Coefficient of Variation.

	<i>Jan.</i>	<i>Feb.</i>	<i>Mar.</i>	<i>Apr.</i>	<i>May</i>	<i>Jun.</i>	<i>Jul.</i>	<i>Aug.</i>	<i>Sep.</i>	<i>Oct.</i>	<i>Nov.</i>	<i>Dec.</i>
CanESM2												
2006–2099 TRMM and Simulation												
Mean	82.4	141.7	297.9	314.1	253.4	153.8	220.3	380.4	323.2	278.9	137.4	42.8
Standard Deviation	86.5	84.6	116.3	63.4	63.0	34.1	117.7	109.2	61.2	88.4	51.6	26.6
CV, %	105.0	59.7	39.0	20.2	24.9	22.2	53.4	28.7	18.9	31.7	37.6	62.3
2006–2065 TRMM and Simulation												
Mean	44.2	99.9	237.5	307.3	225.8	154.5	144.9	322.1	334.5	243.2	144.6	36.2
Standard Deviation	41.9	54.7	74.7	64.0	42.5	34.9	46.0	87.4	65.0	69.2	49.2	14.8
CV, %	94.7	54.8	31.4	20.8	18.8	22.6	31.7	27.1	19.4	28.5	34.0	41.0
2006–2035 TRMM and Simulation												
Mean	27.1	75.3	196.6	289.3	211.9	153.7	114.2	263.1	331.2	224.9	146.4	34.3
Standard Deviation	14.8	42.7	48.5	71.1	47.8	35.6	18.8	67.3	58.3	63.7	48.6	13.1
CV, %	54.7	56.6	24.7	24.6	22.6	23.1	16.5	25.6	17.6	28.3	33.2	38.3
1975–2005 TRMM and Weather Generator												
28.4	32.7	127.7	198.0	200.4	108.6	150.5	172.9	149.1	160.6	79.4	31.8	
Standard Deviation	21.9	20.1	35.3	50.5	35.7	28.1	35.4	38.7	30.5	26.6	29.9	11.8
CV, %	77.2	61.5	27.7	25.5	17.8	25.9	23.5	22.4	20.4	16.6	37.6	37.1
HadCM3												
2006–2097 TRMM and Simulation												
Mean	140.5	160.5	227.2	293.8	180.5	114.4	345.7	179.0	332.0	171.1	54.2	105.3
Standard Deviation	55.1	65.2	73.4	101.6	63.9	29.2	203.7	74.3	119.6	45.0	27.5	42.5
CV, %	39.2	40.6	32.3	34.6	35.4	25.5	58.9	41.5	36.0	26.3	50.8	40.4
2006–2065 TRMM and Simulation												
Mean	120.0	148.6	228.0	269.5	195.9	125.0	229.1	186.0	261.4	180.2	56.9	83.3
Standard Deviation	44.2	63.7	75.0	80.3	49.9	25.8	59.3	86.7	80.8	49.6	32.7	32.8
CV, %	36.9	42.9	32.9	29.8	25.5	20.6	25.9	46.6	30.9	27.5	57.4	39.4
2006–2035 TRMM and Simulation												
Mean	106.4	108.1	172.7	220.2	177.7	121.9	218.1	238.8	231.8	213.3	83.3	76.9
Standard Deviation	50.7	50.5	58.4	79.7	61.3	25.2	27.6	39.9	41.2	27.2	23.4	34.7
CV, %	47.6	46.7	33.8	36.2	34.5	20.7	12.6	16.7	17.8	12.7	28.1	45.1
1975–2005 TRMM and Weather Generator												
Mean	26.4	37.1	132.5	222.1	208.3	112.4	170.7	175.8	158.9	161.3	74.5	33.8
Standard Deviation	19.6	13.7	27.0	31.1	21.6	19.5	9.8	15.9	19.4	18.4	15.4	7.9
CV, %	74.3	36.9	20.4	14.0	10.3	17.3	5.8	9.0	12.2	11.4	20.7	23.3

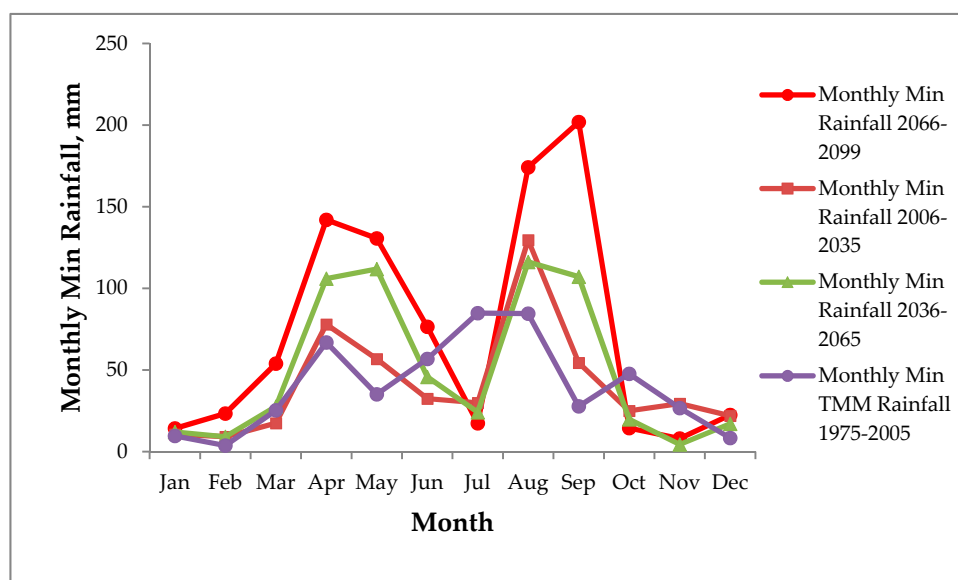
The red and black items show the high CV values. The red color gives the highest CV values for rainfall onset and cessation periods.

Based on CanESM2 rainfall projection, the three months' time scale SPI values show that the long term future rainfall pattern is going to be dominated by wet events (severely wet to extremely wet) as compared to the current and near future situation which is dominated by droughts (moderately dry to extremely dry). Figures 14–16 show the SPI₃ values of 2006–2099 for Kaabong, Agoro and Gulu locations respectively. Tables 9–11 show percentage of variation of SPI values for the period 2006–2099 for Kaabong, Agoro and Gulu locations respectively. The moderately, severely and extremely wet SPI values increase from mid to end of the century compared to the current situation. In Agoro, for example, the percentage of extremely wet SPI values (>2) rise from 0 (2006–2035) to 0.8 (2036–2065) and then to 6.4 (2066–2099). This is in agreement with the high CV values of Kaabong and Agoro, as it is observed in Tables 6 and 7. These results suggest that the semi-arid and semi-humid section

of Aswa catchment will have high rainfall variability in the future. Nicholson, et al. [50] also found that semi-arid climate in Africa are prone to extreme rainfall variability. Batisani and Yarnal [51] and Byakatonda et al. [52] reported increasing rainfall variability in semi-arid Botswana. The expected increased future rainfall variability will have profound impact on various sectors such as agricultural production, water resources, infrastructure and the general environment in Aswa catchment. Droughts will cause crop failure and extreme wet conditions will lead to water logging, flooding and soil erosion, which also affect crop yields negatively. Studies from different parts of the world suggest that high rainfall events can lead to crop yield reduction. Studies from Ghana revealed negative impact on crop yields due to heavy rainfall events [53,54].

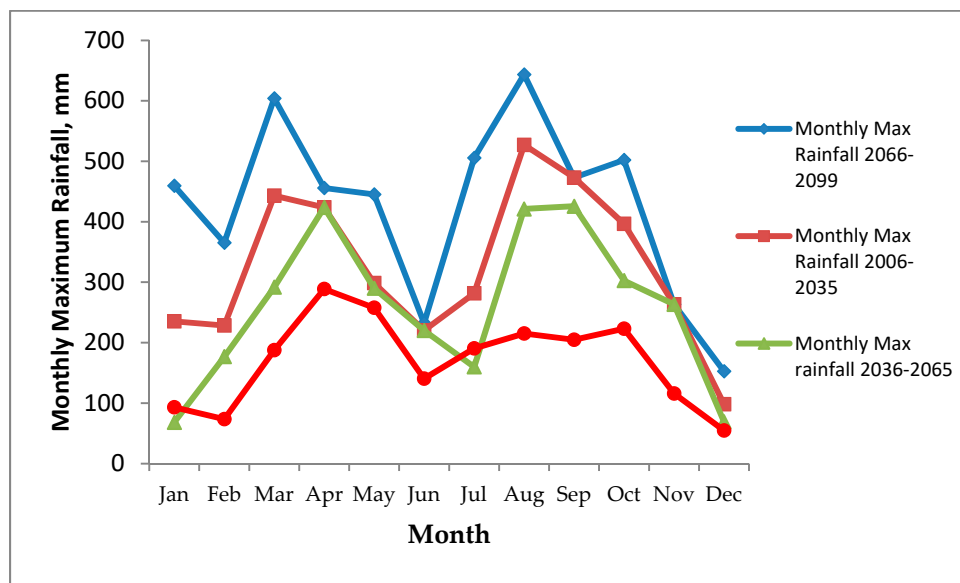


(a)

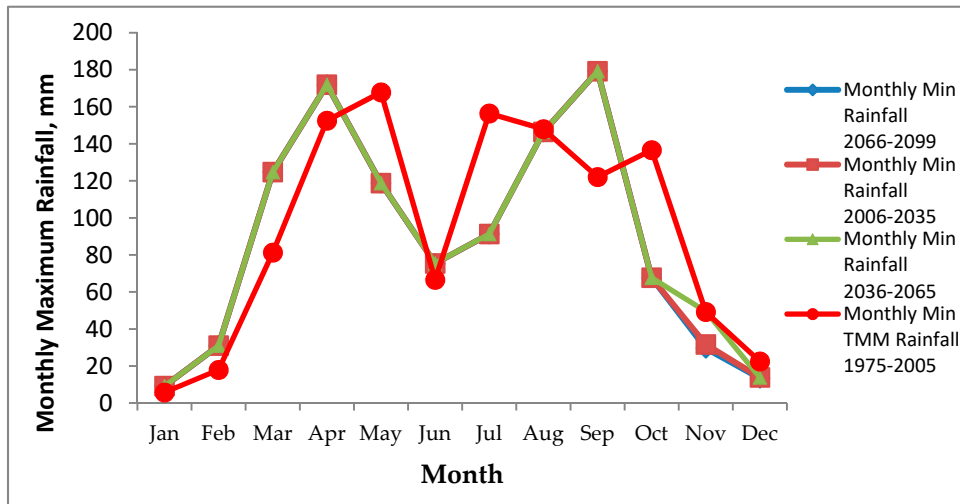


(b)

Figure 12. Agoro CanESM2 future average monthly rainfall variations for (a) maximum monthly rainfall and (b) minimum monthly rainfall.



(a)



(b)

Figure 13. Gulu CanESM2 future average monthly rainfall variations for (a) maximum monthly rainfall and (b) minimum monthly rainfall.

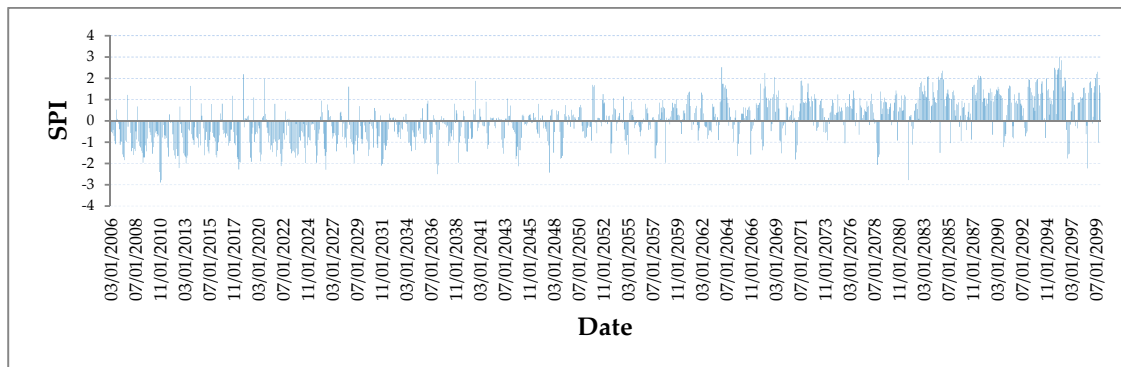


Figure 14. CanESM2 3-month period SPI values for Kaabong for the duration 2006–2099.

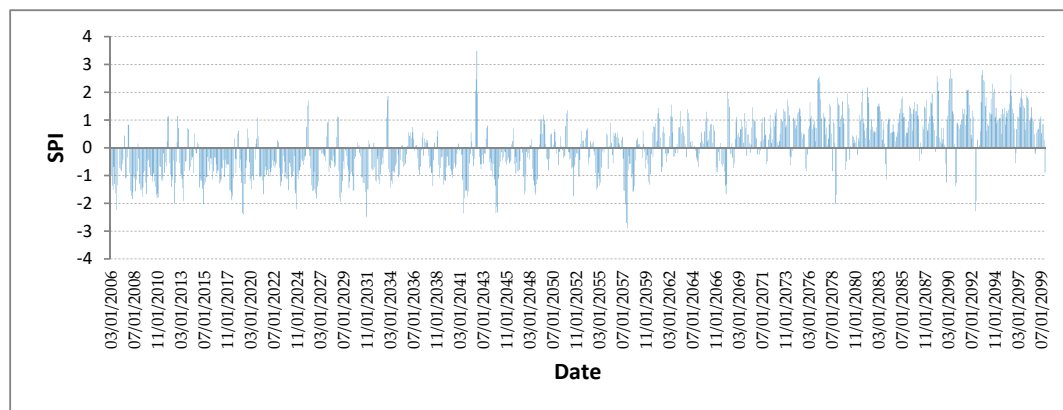


Figure 15. CanESM2 3-month period SPI values for Agoro for the duration 2006–2099.

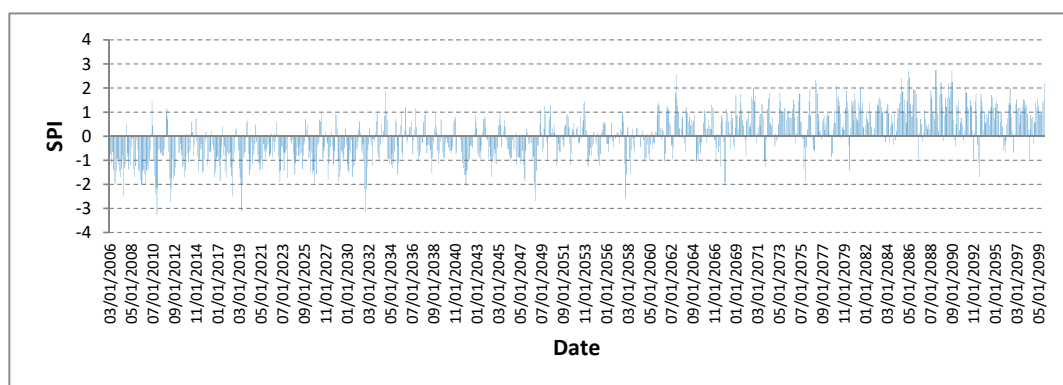


Figure 16. CanESM2 3-month period SPI values for Gulu for the duration 2006–2099.

Table 9. Percentage variation of Standardized Precipitation Index (SPI) values for Kaabong over the period 2006–2099.

SPI		Time Period		
Value	Class	2006–2035	2036–2065	2066–2099
Percentage of period				
≥2	Extremely Wet	0.3	0.3	5.4
1.5 to 1.99	Severely Wet	0.8	2.5	11.0
1.0 to 1.49	Moderately Wet	0.8	2.8	22.8
0.99 to −0.99	Mildly wet/dry (near normal)	63.4	83.6	55.4
−1.0 to −1.49	Moderately Dry	19.0	5.8	2.5
−1.5 to −2.0	Severely Dry	12.8	3.6	2.2
≤−2.0	Extremely Dry	2.8	1.4	0.7
Maximum SPI Value		2.2	2.5	3.0
Minimum SPI Value		−2.9	−2.5	−2.8

Table 10. Percentage variation of SPI values for Agoro over the period 2006–2099.

SPI		Time Period		
Value	Class	2006–2035	2036–2065	2066–2099
Percentage of period				
≥2	Extremely Wet	0.0	0.8	6.4
1.5 to 1.99	Severely Wet	1.1	0.6	9.8
1.0 to 1.49	Moderately Wet	2.0	4.4	24.8
0.99 to −0.99	Mildly wet/dry (near normal)	62.0	80.8	56.4
−1.0 to −1.49	Moderately Dry	22.9	6.9	1.5
−1.5 to −2.0	Severely Dry	10.1	4.4	0.7
≤−2.0	Extremely Dry	2.0	1.9	0.5
Maximum SPI Value		1.87	3.48	3.0
Minimum SPI Value		−2.48	−2.9	−2.28

Table 11. Percentage variation of SPI values for Gulu over the period 2006–2099.

SPI		Time Period		
Value	Class	2006–2035 Percentage of period	2036–2065	2066–2099
≥2	Extremely Wet	0.0	0.1	1.9
1.5 to 1.99	Severely Wet	0.3	0.4	4.6
1.0 to 1.49	Moderately Wet	0.8	3.1	10.5
0.99 to −0.99	Mildly wet/dry (near normal)	64.5	73.3	67.3
−1.0 to −1.49	Moderately Dry	20.4	14.3	9.8
−1.5 to −2.0	Severely Dry	10.1	6.3	4.3
≤−2.0	Extremely Dry	3.9	2.5	1.7
Maximum SPI Value		1.9	2.5	2.8
Minimum SPI Value		−3.3	−3.3	−3.3

4. Discussion

Due to scarce and inconsistent station rainfall data in Aswa catchment, secondary data from TRMM was used to downscale two GCMs (CanEMS2 and HadEM3) for investigating likely future rainfall quantities, variability onset and cessation of rainfall months for this study. However, secondary data from satellite sometimes present challenges of non-homogeneity [27] and week correlation with the actual recorded data. The intervention tests show that the TRMM data is homogeneous. The correction between TRMM and the limited recorded rainfall data in Aswa catchment show a coefficient of determination, R^2 value of 0.65 ($R = 0.806$), which gives confidence of using the TRMM rainfall data as proxy for station data. The biases are generally low with an average of 1.018. TRMM rainfall validation studies carried out in Ghana [31] revealed similar bias values ranging from 1.047 to 1.479. The good correlation between station and TRMM rainfall and minimal bias between downscaled and TRMM rainfall are deemed sufficient to allow for use of TRMM rainfall in the absence of station rainfall data for simulation of future scenarios. The downscaled simulated future rainfall using SDSM, CanEMS2 and HadEM3 CGM predictors show increased rainfall in the future. In reference to the SDSM calibration results, we expect CanESM2 (with higher R^2 values) based simulated future rainfall data for Aswa catchment to be more accurate than HadCM3 based data. The correlation coefficients for CanESM2 are marginally higher and the standard errors are lower than for HadCM3 (Table 3).

The results of Man Kendal tau values are positive, as can be seen for example, for Agoro and Amuria locations ranging from 0.172 to 0.683 (Table 5). This suggests a strong positive trend in the future. Agoro represents the semi humid section and Amuria represents the humid section of the catchment. This trend is expected to become steeper as we move from mid (2036–2065) to end of the century (2066–2099). These results are also supported by the SPI values, which can be seen from Figure 14, Figure 15, Figure 16, Tables 9–11. The percentage of SPI values greater than 1.5 (severely wet and extremely wet) are to increase as we move to mid and end of the century. This suggests that the future rainfall is not only expected to increase but also have extremely wet patterns, which are likely to affect crop production, infrastructure and the environment negatively.

The expected increase in rainfall trend could be good for improving crop yields in an area such as the Aswa catchment, which has been suffering from droughts and water stress. However, analysis of the rainfall patterns show increased and high monthly CV values in the future. CV values above 30% suggest high variability and poor rainfall distribution. The CV values, as can be seen from Tables 6–8 for Agoro, Kaabong and Gulu locations respectively, are high reaching up to 118.5%. The onset and cessation months of February–April and October–November respectively show the highest rainfall variability. The rainfall patterns during these months are expected to become more unreliable as we move to mid century to end of the century. The CV values for future simulated rainfall data based on CanESM2 are generally higher than for the data sets based on HadCM3. However, looking at the higher correlation coefficients for CanESM2 data sets during calibration and validation, we consider the corresponding CV values for the data sets to be more reliable.

The analysis of future rainfall onset and cessation dates results also support the indications of the CV. Figures 4–11 show the variation of future rainfall onset and cessation dates for Agago (humid) and Kaabong (semi-arid) locations for CanESM2 and HadCM3 based downscaling using both rainfall and rainy days data. The future rainfall onset and cessation dates are expected to come earlier and later than the current dates by up to four and five weeks respectively. For Agago the future rainfall onset is expected to come in February instead of March and cessation is expected in November instead of late October as is currently being experienced. For Kaabong, future rainfall onset is expected to come late February/early March instead of late March as is currently happening, while the future cessation is expected in November instead of the current late October. The two GCM gave similar results for each location. The change in rainfall onset and cessation dates is likely to affect the farming activities of the peasant farmers and crop yields.

5. Conclusions

In this study, we examined the future changes in rainfall patterns, trends, extreme occurrences, onset and cessation of rainfall over Aswa catchment using SPI, Mann–Kendall statistics, descriptive statistics (coefficient of variability), and cumulative percentage mean rainfall methods to provide insight into near future (2006–2035), midterm (2036–2065) and long term (2066–2100) future periods.

The results suggest that annual rainfall over Aswa catchment is going to increase especially in the mid and long term future by up to 100%, and even more. This could be a good development for the farmers if the rainfall turns out to be reliable and well distributed. However, the future presents a highly variable and unreliable rainfall pattern. This can be seen from the high CV (up by 118.5%) and the rise in percentage of SPI values for extremely wet periods. The study reveals SPI values for extremely wet periods increasing from zero in (2006–2035), to 0.8 in (2036–2065) and to 6.4 in (2066–2099) periods for Agoro which lies in the semi-humid region of the catchment. For Kaabong located in the semi-arid region of the catchment, the rise in percentage of SPI values for extremely wet periods is 0.3, 0.3 and 5.4 respectively. For Gulu located in the humid region of the catchment, is from 0 to 0.1 to 1.9 respectively. This suggests that the semi-arid and semi-humid regions of the catchment will experienced more extremely wet conditions in the future compared to the humid region. Extremely dry periods are, however, expected to reduce although they will continue to be experienced as can be seen from Tables 9–11.

The onset and cessation of rain are also expected to shift backwards and forward by up to four and five weeks respectively. This in turn is expected to affect farming activities such as field preparation, planting and harvesting. The future scenarios are increased, highly variable and unreliable rainfall in Aswa catchment, with the drier semiarid section being the most affected. This may result in floods, water logging, severe soil erosion and even droughts with consequent reduction in crop yields and negative impact on the livelihood of the farmers. These changes can affect the future agricultural production, water availability, environment and socio-economic wellbeing over the Aswa catchment. The results of the study can be of use for future catchment water resources planning and management, agricultural and socio-economic planning, and introduction of appropriate mitigation measures such as provision of supplementary irrigation, introduction of new crop varieties/farming system, soil and water conservation measures, drainage and reservoir development.

Author Contributions: Conceptualization, M.I., P.T.O., B.P.P. and D.B.M.; Formal analysis, M.I.; Investigation, M.I.; Methodology, M.I.; Resources, P.T.O., B.P.P. and D.B.M.; Supervision P.T.O., B.P.P. and D.B.M.; Validation M.I., P.T.O., B.P.P. and D.B.M.; Visualization, M.I.; Writing—original draft, M.I., P.T.O., B.P.P. and D.B.M.; Writing—review & editing M.I., P.T.O., B.P.P. and D.B.M. All authors have read and agreed to the published version of the manuscript.

Funding: This research received no external funding.

Acknowledgments: This study was made possible by the sponsorship of EU's Intra Africa Mobility to Enhance Training of Engineering Graduates in Africa (METEGA) Program at University of Botswana. The authors wish to acknowledge NASA for providing free TRMM satellite data listed in Table 1 of this paper. We would like to thank the developers of SDSM for providing this model for free. The authors also would like to acknowledge the limited available rainfall data for Aswa catchment provided by the Directorate of Water Resource Development (DWRD),

Uganda. We would like to thank the University of Botswana for provision of funds through the Office of Research and Development (ORD) for data acquisition.

Conflicts of Interest: The authors declare no conflict of interest.

References

1. Mukherjee, S.; Aadhar, S.; Stone, D.; Mishra, V. Increase in extreme precipitation events under anthropogenic warming in India. *Weather. Clim. Extremes* **2018**, *20*, 45–53. [\[CrossRef\]](#)
2. Lehmanni, J.; Coumou, D.; Frieler, K. Increased record-breaking precipitation events under global warming. *Clim. Chang.* **2015**, *132*, 501–515. [\[CrossRef\]](#)
3. O’Gorman, P.A. Precipitation Extremes Under Climate Change. *Curr. Clim. Chang. Rep.* **2015**, *1*, 49–59. [\[CrossRef\]](#) [\[PubMed\]](#)
4. Kharin, V.V.; Zwiers, F.W.; Zhang, X.; Wehner, M. Changes in temperature and precipitation extremes in the CMIP5 ensemble. *Clim. Chang.* **2013**, *119*, 345–357. [\[CrossRef\]](#)
5. Schewe, J.; Heinke, J.; Gerten, D.; Haddeland, I.; Arnell, N.W.; Clark, D.B.; Dankers, R.; Eisner, S.; Fekete, B.M.; Colon-Gonzalez, F.J.; et al. Multimodel assessment of water scarcity under climate change. *Proc. Natl. Acad. Sci. USA* **2014**, *111*, 3245–3250. [\[CrossRef\]](#) [\[PubMed\]](#)
6. IPCC. Summary for Policymakers. In *Global Warming of 1.5 °C; An IPCC Special Report on the Impacts of Global Warming of 1.5 °C above Pre-Industrial Levels and Related Global Greenhouse Gas Emission Pathways, in the Context of Strengthening the Global Response to the Threat of Climate Change*; Masson-Delmotte, V., Zhai, P., Pörtner, H.O., Roberts, D., Skea, J., Shukla, P.R., Pirani, A., Moufouma-Okia, W., Péan, C., Pidcock, R., et al., Eds.; World Meteorological Organization: Geneva, Switzerland, 2018; p. 32.
7. Recha, C.W.; Makokha, G.L.; Traore, P.C.S.; Shisanya, C.; Lodoun, T.; Sako, A. Determination of seasonal rainfall variability, onset and cessation in semi-arid Tharaka district, Kenya. *Theor. Appl. Clim.* **2011**, *108*, 479–494. [\[CrossRef\]](#)
8. Traore, B.; Corbeels, M.; Van Wijk, M.; Rufino, M.C.; Giller, K.E. Effects of climate variability and climate change on crop production in southern Mali. *Eur. J. Agron.* **2013**, *49*, 115–125. [\[CrossRef\]](#)
9. Sultan, B.; Roudier, P.; Quirion, P.; Alhassane, A.; Müller, B.; Dingkuhn, M.; Ciais, P.; Guimberteau, M.; Traore, S.; Baron, C. Assessing climate change impacts on sorghum and millet yields in the Sudanian and Sahelian savannas of West Africa. *Environ. Res. Lett.* **2013**, *8*, 014040. [\[CrossRef\]](#)
10. Omoyo, N.N.; Wakhungu, J.; Oteng’I, S. Effects of climate variability on maize yield in the arid and semi arid lands of lower eastern Kenya. *Agric. Food Secur.* **2015**, *4*, 881. [\[CrossRef\]](#)
11. Adhikari, U.; Nejadhashemi, A.; Woznicki, S.A. Climate change and eastern Africa: A review of impact on major crops. *Food Energy Secur.* **2015**, *4*, 110–132. [\[CrossRef\]](#)
12. Fishman, R. More uneven distributions overturn benefits of higher precipitation for crop yields. *Environ. Res. Lett.* **2016**, *11*, 24004. [\[CrossRef\]](#)
13. Wanyama, J.; Ssegane, H.; Kisekka, I.; Komakech, A.J.; Banadda, N.; Zziwa, A.; Ebong, T.O.; Mutumba, C.; Kiggundu, N.; Kayizi, R.K.; et al. Irrigation Development in Uganda: Constraints, Lessons Learned, and Future Perspectives. *J. Irrig. Drain. Eng.* **2017**, *143*, 04017003. [\[CrossRef\]](#)
14. UBOS. *National Population and Housing Census 2014*; Uganda Bureau of Statistics (UBOS): Kampala, Uganda, 2014.
15. Iwadra, M.; Odirile, P.T.; Parida, B.P.; Moalafhi, D.B. Evaluation of future climate using SDSM and secondary data (TRMM and NCEP) for poorly gauged catchments of Uganda: The case of Aswa catchment. *Theor. Appl. Clim.* **2018**, *137*, 2029–2048. [\[CrossRef\]](#)
16. Kenabatho, P.K.; Parida, B.; Moalafhi, D. Evaluation of satellite and simulated rainfall products for hydrological applications in the Notwane catchment, Botswana. *Phys. Chem. Earth* **2017**, *100*, 19–30. [\[CrossRef\]](#)
17. Maraun, D. Bias Correcting Climate Change Simulations—A Critical Review. *Curr. Clim. Chang. Rep.* **2016**, *2*, 211–220. [\[CrossRef\]](#)
18. Zickfeld, K.; Eby, M.; Weaver, A.J.; Alexander, K.; Crespin, E.; Edwards, N.R.; Eliseev, A.V.; Feulner, G.; Fichet, T.; Forest, C.E.; et al. Long-Term Climate Change Commitment and Reversibility: An EMIC Intercomparison. *J. Clim.* **2013**, *26*, 5782–5809. [\[CrossRef\]](#)

19. Hossain, I.; Rasel, H.M.; Alam Imteaz, M.; Mekanik, F. Long-term seasonal rainfall forecasting using linear and non-linear modelling approaches: A case study for Western Australia. *Theor. Appl. Clim.* **2019**, *132*, 131–141. [\[CrossRef\]](#)
20. Abbot, J.; Marohasy, J. Skilful rainfall forecasts from artificial neural networks with long duration series and single-month optimization. *Atmos. Res.* **2017**, *197*, 289–299. [\[CrossRef\]](#)
21. Huang, J.; Zhang, J.; Zhang, Z.; Xu, C.-Y.; Wang, B.; Yao, J. Estimation of future precipitation change in the Yangtze River basin by using statistical downscaling method. *Stoch. Environ. Res. Risk Assess.* **2010**, *25*, 781–792. [\[CrossRef\]](#)
22. Fotso-Nguemo, T.C.; Vondou, D.A.; Pokam, W.M.; Djomou, Z.Y.; Diallo, I.; Haensler, A.; Tchotchou, L.A.D.; Kamsu-Tamo, P.H.; Gaye, A.T.; Tchawoua, C. On the added value of the regional climate model REMO in the assessment of climate change signal over Central Africa. *Clim. Dyn.* **2017**, *49*, 3813–3838. [\[CrossRef\]](#)
23. Mehrotra, R.; Sharma, A. A Multivariate Quantile-Matching Bias Correction Approach with Auto- and Cross-Dependence across Multiple Time Scales: Implications for Downscaling. *J. Clim.* **2016**, *29*, 3519–3539. [\[CrossRef\]](#)
24. Moalafhi, D.B.; Sharma, A.; Evans, J.; Mehrotra, R.; Rocheta, E. Impact of bias-corrected reanalysis-derived lateral boundary conditions on WRF simulations. *J. Adv. Model. Earth Syst.* **2017**, *9*, 1828–1846. [\[CrossRef\]](#)
25. Sangelantoni, L.; Russo, A.; Gennaretti, F. Impact of bias correction and downscaling through quantile mapping on simulated climate change signal: A case study over Central Italy. *Theor. Appl. Clim.* **2018**, *135*, 725–740. [\[CrossRef\]](#)
26. Mahmood, R.; Babel, M.S. Future changes in extreme temperature events using the statistical downscaling model (SDSM) in the trans-boundary region of the Jhelum river basin. *Weather. Clim. Extremes* **2014**, *5*, 56–66. [\[CrossRef\]](#)
27. Saha, S.; Moorthi, S.; Wu, X.; Wang, J.; Nadiga, S.; Tripp, P.; Behringer, D.; Hou, Y.-T.; Chuang, H.-Y.; Iredell, M.; et al. The NCEP Climate Forecast System Version 2. *J. Clim.* **2014**, *27*, 2185–2208. [\[CrossRef\]](#)
28. Babel, M.S.; Turyatunga, E. Evaluation of climate change impacts and adaptation measures for maize cultivation in the western Uganda agro-ecological zone. *Theor. Appl. Clim.* **2014**, *119*, 239–254. [\[CrossRef\]](#)
29. Mekonnen, D.F.; Disse, M. Analyzing the future climate change of Upper Blue Nile River basin using statistical downscaling techniques. *Hydrol. Earth Syst. Sci.* **2018**, *22*, 2391–2408. [\[CrossRef\]](#)
30. Hasan, D.S.N.A.B.P.A.; Ratnayake, U.; Shams, S.; Nayan, Z.B.H.; Rahman, E.K.A. Prediction of climate change in Brunei Darussalam using statistical downscaling model. *Theor. Appl. Clim.* **2017**, *133*, 343–360. [\[CrossRef\]](#)
31. Amekudzi, L.K.; Osei, M.A.; Atiah, W.A.; Aryee, J.; Ahiataku, M.A.; Quansah, E.; Preko, K.; Danuor, S.K.; Fink, A.H. Validation of TRMM and FEWS Satellite Rainfall Estimates with Rain Gauge Measurement over Ashanti Region, Ghana. *Atmos. Clim. Sci.* **2016**, *6*, 500–518. [\[CrossRef\]](#)
32. Amekudzi, L.K.; Yamba, E.I.; Preko, K.; Asare, E.O.; Aryee, J.; Baidu, M.; Codjoe, S.N.A. Variabilities in Rainfall Onset, Cessation and Length of Rainy Season for the Various Agro-Ecological Zones of Ghana. *Climate* **2015**, *3*, 416–434. [\[CrossRef\]](#)
33. Odekunle, T.O. Determining rainy season onset and retreat over Nigeria from precipitation amount and number of rainy days. *Theor. Appl. Clim.* **2005**, *83*, 193–201. [\[CrossRef\]](#)
34. Odekunle, T.O.; Balogun, E.E.; Ogunkoya, O.O. On the prediction of rainfall onset and retreat dates in Nigeria. *Theor. Appl. Clim.* **2005**, *81*, 101–112. [\[CrossRef\]](#)
35. Guenang, G.M.; Kamga, F.M. Onset, retreat and length of the rainy season over Cameroon. *Atmos. Sci. Lett.* **2012**, *13*, 120–127. [\[CrossRef\]](#)
36. Ngetich, F.K.; Mucheru-Muna, M.; Mugwe, J.; Shisanya, C.; Diels, J.; Mugendi, D. Length of growing season, rainfall temporal distribution, onset and cessation dates in the Kenyan highlands. *Agric. For. Meteorol.* **2014**, *188*, 24–32. [\[CrossRef\]](#)
37. Mugalavai, E.M.; Kipkorir, E.C.; Raes, D.; Rao, M.S. Analysis of rainfall onset, cessation and length of growing season for western Kenya. *Agric. For. Meteorol.* **2008**, *148*, 1123–1135. [\[CrossRef\]](#)
38. Akinseye, F.M.; Agele, S.O.; Traore, P.C.S.; Adam, M.; Whitbread, A.M. Evaluation of the onset and length of growing season to define planting date—‘a case study for Mali (West Africa)’. *Theor. Appl. Clim.* **2015**, *124*, 973–983. [\[CrossRef\]](#)
39. Odekunle, T.O. Rainfall and the length of the growing season in Nigeria. *Int. J. Clim.* **2004**, *24*, 467–479. [\[CrossRef\]](#)

40. Kallis, G. Droughts. *Annual Review of Environment and Resources*. *Annu. Rev.* **2008**, *33*, 85–118. [[CrossRef](#)]
41. Tirivarombo, S.; Osupile, D.; Eliasson, P. Drought monitoring and analysis: Standardised Precipitation Evapotranspiration Index (SPEI) and Standardised Precipitation Index (SPI). *Phys. Chem. Earth* **2018**, *106*, 1–10. [[CrossRef](#)]
42. Kumar, A. Characterizing meteorological drought using standardized precipitation index for Dehradun, Uttarakhand. *Indian J. Soil Conserv.* **2016**, *44*, 157–162. [[CrossRef](#)]
43. McKee, T.B.; Doesken, N.J.; Kleist, J. The Relationship of Drought Frequency and Duration to Time Scales. In Proceedings of the Eighth Conference on Applied Climatology, Anaheim, CA, USA, 17–22 January 1993.
44. Guenang, G.M.; Kamga, F.M. Computation of the Standardized Precipitation Index (SPI) and Its Use to Assess Drought Occurrences in Cameroon over Recent Decades. *J. Appl. Meteorol. Clim.* **2014**, *53*, 2310–2324. [[CrossRef](#)]
45. Yusof, F.; Hui-Mean, F.; Suhaila, J.; Yusop, Z.; Ching-Yee, K.; Jamaludin, S.S.S. Rainfall characterisation by application of standardised precipitation index (SPI) in Peninsular Malaysia. *Theor. Appl. Clim.* **2013**, *115*, 503–516. [[CrossRef](#)]
46. Bari, S.H.; Rahman, T.U.; Hoque, M.A.; Hussain, M. Analysis of seasonal and annual rainfall trends in the northern region of Bangladesh. *Atmos. Res.* **2016**, 148–158. [[CrossRef](#)]
47. Shefine, B.G. Analysis of Meteorological Drought Using SPI and Large Scale Climate Variability (ENSO)-A case study in North Shewa Zone, Amhara Regional State, Ethiopia. *Hydrol. Curr. Res.* **2018**, *9*. [[CrossRef](#)]
48. Karanja, A.; Ondimu, K.; Recha, C. Analysis of Temporal Drought Characteristic Using SPI Drought Index Based on Rainfall Data in Laikipia West Sub-County, Kenya. *OALib* **2017**, *4*, 1–11. [[CrossRef](#)]
49. Kisaka, M.O.; Mucheru-Muna, M.; Ngetich, F.K.; Mugwe, J.; Mugendi, D.; Mairura, F. Rainfall Variability, Drought Characterization, and Efficacy of Rainfall Data Reconstruction: Case of Eastern Kenya. *Adv. Meteorol.* **2015**, *2015*, 1–16. [[CrossRef](#)]
50. Nicholson, S.E.; Funk, C.; Fink, A.H. Rainfall over the African continent from the 19th through the 21st century. *Glob. Planet. Chang.* **2018**, *165*, 114–127. [[CrossRef](#)]
51. Batisani, N.; Yarnal, B. Rainfall variability and trends in semi-arid Botswana: Implications for climate change adaptation policy. *Appl. Geogr.* **2010**, *30*, 483–489. [[CrossRef](#)]
52. Byakatonda, J.; Parida, B.; Kenabatho, P.; Moalafhi, D. Modeling dryness severity using artificial neural network at the Okavango Delta, Botswana. *Glob. Nest. J.* **2016**, *18*, 463–481.
53. Ibn Musah, A.-A.; Du, J.; Udimal, T.B.; Sadick, M.A. The Nexus of Weather Extremes to Agriculture Production Indexes and the Future Risk in Ghana. *Climate* **2018**, *6*, 86. [[CrossRef](#)]
54. Derbile, E.K.; Kasei, R.A. Vulnerability of crop production to heavy precipitation in north-eastern Ghana. *Int. J. Clim. Chang. Strat. Manag.* **2012**, *4*, 36–53. [[CrossRef](#)]



© 2020 by the authors. Licensee MDPI, Basel, Switzerland. This article is an open access article distributed under the terms and conditions of the Creative Commons Attribution (CC BY) license (<http://creativecommons.org/licenses/by/4.0/>).